All-Solution Processed, Highly Stable MXene/Cu Nanowire Networks for Flexible Transparent Thin Film Heaters

Journal:	*ACS Applied Nano Materials*
Manuscript ID	an-2023-05027b.R2
Manuscript Type:	Article
Date Submitted by the Author:	31-Oct-2023
Complete List of Authors:	Çetin, Öykü; Orta Dogu Teknik Universitesi, Metallurgical and Materials ENGINEERING Cakir, Onuralp; Orta Dogu Teknik Universitesi, METALLURGICAL AND MATERIALS ENGINEERING KOYLAN, SERKAN; KU Leuven Doganay, Doga; Orta Dogu Teknik Universitesi, METALLURGICAL AND MATERIALS ENGINEERING Khan, Yaqoob; Middle East Technical University Unalan, Husnu; Orta Dogu Teknik Universitesi, METALLURGICAL AND MATERIALS ENGINEERING

All-Solution Processed, Highly Stable MXene/Cu Nanowire Networks for Flexible Transparent Thin Film Heaters

Oyku Cetin[1], Onuralp Cakir[1], Serkan Koylan[2,3], Doga Doganay[1], Yaqoob Khan[1] and Husnu Emrah Unalan[1,*]

[1] Department of Metallurgical and Materials Engineering, Middle East Technical University (METU), 06800, Ankara, Turkey

[2] Quantum Solid State Physics (QSP), KU Leuven, Celestijnenlaan 220D, Leuven 3001, Belgium

[3] imec, Kapeldreef 75, Leuven 3001, Belgium

Abstract

Copper nanowire (Cu NW) networks are recognized for their excellent electrical conductivity and cost-effectiveness, making them a prime choice for transparent conductors. However, their susceptibility to degradation presents a significant challenge in various applications. In this study, we explore the efficacy of incorporating Ti_3C_2 MXene into copper nanowire (MXene/Cu NW) networks to enhance the stability and performance of Cu NW-based transparent conducting electrodes (TCEs). The results showed that the electrical resistance of bare Cu NW networks rapidly increased within 10 days under ambient conditions, whereas the deposition of Ti_3C_2 MXene enhanced the stability of the networks up to 10 months under ambient conditions. A significant figure of merit (FoM) of 109 was achieved from the MXene/Cu NW networks, compared to only 69 for bare Cu NW networks. The fabricated TCEs also showcased their long-term stability when utilized as transparent thin film heaters (TTFH). The TTFHs utilizing MXene/Cu NW networks displayed consistent performance over the course of one week when subjected to a bias of 3 V. Furthermore, the TTFHs have also been utilized as flexible human thermotherapy patches and defrosting networks. Our research underscores the potential of MXene/Cu NW electrodes in optoelectronic applications where both high FoM and long-term stability are essential, thereby expanding the possibilities for cost-effective TCEs in a variety of applications.

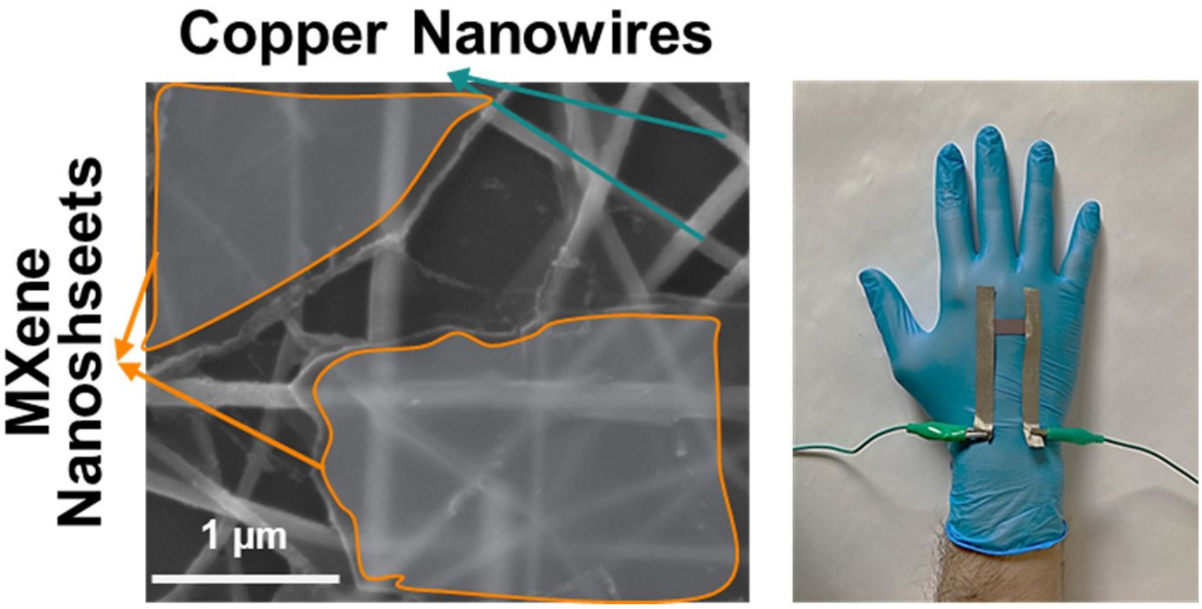

Keywords: Copper Nanowires, Transparent Conductors, Ti_3C_2 MXene, Oxidation Stability, Transparent Thin Film Heaters, Thermotherapy

* Corresponding Autor: unalan@metu.edu.tr

INTRODUCTION

Transparent conducting electrodes (TCEs) gained significant importance across various fields, serving a wide range of applications, including photovoltaics[1], light emitting diodes (LEDs)[2], touch screens[3], electrochromic windows[4], sensors[5] and transparent heaters[6]. Indium tin oxide (ITO) is the mainstream material used in these optoelectronic applications[7]. Despite having a well-established production infrastructure and forming a benchmark for optoelectronic performance[8], the scarcity of indium in the Earth's crust[9] drives its price upwards. Moreover, the full utilization of ITO is hampered by manufacturing limitations in conjunction with its inherent brittleness[10]. As a result, it is crucial to thoroughly investigate and incorporate alternative materials to effectively address and overcome these challenges. The research in the past decade proved that alternative materials such as metal nanowires[11], carbon nanotubes (CNTs)[12], graphene and reduced graphene oxide (rGO)[13], and thin layers of transition metal carbides, nitrides, or carbonitrides (MXenes)[14] have the potential to be utilized as transparent conducting networks. Among them, metallic nanowires demonstrated significant potential as a substitute for ITO due to their comparable optoelectronic capabilities, including excellent optical transmittance and electrical conductivity. Furthermore, the superior flexibility of metallic nanowires renders them ideal alternatives for next-generation applications like wearable and flexible electronics. Among metal nanowires, silver nanowires (Ag NWs) have found wide range of applications in transparent heaters[15], textile-based electronics[16], sensors[17] and triboelectric nanogenerators[18,19]. However, as the cost of bulk silver continues to rise, so does the cost of the salts used for Ag NW synthesis, creating a growing demand for more cost-effective alternative technologies.

Copper nanowires (Cu NWs) emerged as competitors to Ag NWs with similar electrical conductivity and optical transmittance[20]. Studies have revealed that the amount of elemental copper in the Earth's crust is 700 times greater than elemental silver and all costs considered copper remains 100 times cheaper than silver[21,22]. Moreover, Cu NWs exhibit mechanical stability similar to Ag NWs when deposited on a variety of flexible, stretchable or bendable substrates[23]. Therefore, Cu NWs can be a promising alternative to Ag NWs in applications that demand robust optoelectronic performance and mechanical stability once the concern of Cu NWs' oxidation instability is successfully resolved. Additionally, it is essential to note that the use of bare Cu NW networks as transparent conducting electrodes (TCEs) in display applications is limited by their inherent reddish hue, which is considered undesirable for such applications[24]. The limited oxidation stability and visual limitations posed by the appearance of the networks restrict the potential application areas for Cu NW-based electronics.

To overcome the stability issue regarding Cu NW networks, different approaches have been developed, such as the fabrication of core-shell structures[25,26], deposition of a protective coating layer with metal oxides/sulfides/hydroxide[27,28], carbonaceous materials[29] and polymers[30]. Deposition of metallic shell layers onto nanowires to obtain core-shell layers such as Cu-Ni[31], Cu-Ag[32], Cu-Au[33], Cu-Sn[34], Cu-Zn[35] and Cu-Pt[36] are conducted through solution-based fabrication methods. However, Cu NWs are prone to degradation due to their inherent instability when exposed to aqueous and corrosive reaction media. This vulnerability is particularly pronounced during the solution-based fabrication of core-shell metal nanowires. Additionally, conformal deposition and thickness control of the metallic shell layer is not easily achieved, which may result in unpredictable TCE performance in optoelectronic applications. Moreover, solution-based fabrication methods for core-shell metal nanowires typically exhibit a low yield and involve time-consuming procedures. An alternative approach to addressing the stability issues of Cu NW networks involves depositing protective layers of metal oxides, sulfides, or hydroxides onto the nanowires[25]. Fluorine-doped tin oxide (FTO)[37], aluminum-doped zinc oxide (AZO)[38], zinc oxide (ZnO)[38], and aluminum oxide (Al_2O_3)[39] are deposited by vacuum systems such as atomic layer deposition (ALD)[20]. Fabrication routes involving vacuum systems require a substantial capital investment and restrict the mass production of TCEs[40]. Carbonaceous coating materials are also widely used as protective layers on Cu NW networks. Common carbonaceous protective coating layers include carbon nanotubes (CNTs), graphene, reduced graphene oxide (rGO) and fluorene[41]. The production of carbonaceous protective layer materials, such as graphene, requires the use of vacuum systems operating at high temperatures, leading to the oxidation of copper[42]. On the other hand, solution-based methods such as the Hummers method generate large amounts of hazardous waste for the environment[43]. Polymers are also used to increase the oxidation resistance of metal nanowire networks, where the electrical conductivity of the networks is proved to diminish in the presence of an insulator polymer[30], and polymers are found to provide only a limited level of protection as they degrade when exposed to moisture [25].

Herein, we demonstrated using Ti_3C_2 MXene as a protection layer on Cu NW networks. The synthesis of nanomaterials and their deposition are successfully achieved using simple and efficient solution-based methods. The deposition of Ti_3C_2 MXene nanosheets onto Cu NW networks serves a dual purpose: it acts as a sacrificial protective layer for the Cu NW network while simultaneously enhancing the electrical conductivity of the electrode. Remarkably, this process results in minimal alterations to the optical transmittance of the electrode. The long-term stability of MXene/Cu NW electrodes is evaluated under various conditions, including ambient conditions, high levels of relative humidity and elevated temperatures. With their simple fabrication and excellent oxidation stability, fabricated MXene/Cu NW electrodes constitute strong candidates for highly stable TCEs. The fabricated electrodes are utilized as transparent thin film heaters (TTFHs), demonstrating the versatility of the MXene/Cu NW electrodes in human thermotherapy and defrosting applications with their long-term heating performance.

EXPERIMENTAL

Synthesis of Cu NWs

The hydrothermal synthesis of Cu NWs followed our previously published methods, with minor modifications made for optimization purposes[27,30]. In the synthesis, 5.96 mM of hexadecylamine (HDA) ($C_{16}H_{35}N$, ≥ 94.0 % (a/a), Sigma-Aldrich, USA), 2.22 mM of D-(+)-glucosemonohydrate (Anhydrous, 97.5−102.0 %, Sigma-Aldrich, USA), and 0.98 mM of copper (II) chloride dihydrate ($CuCl_2 \cdot 2H_2O$, ≥ 99.0 %, Sigma-Aldrich, USA) was added into a glass beaker along with 80 ml deionized (DI) water (18.3 MΩ). The mixture was left to stir overnight until a homogeneous mixture was obtained. The solution was moved into a 100 ml Teflon-lined steel autoclave and hydrothermal synthesis of Cu NWs took place in an oven at 105 °C for 18 hours. Later, as synthesized Cu NWs were purified. During the purification process, the mixture obtained from hydrothermal synthesis was centrifuged with DI water several times until the supernatant became clear. A two-phase separation method with chloroform was used to separate the Cu NWs from Cu nanoparticles. The separated nanowires were centrifuged with 2 wt. % of polyvinylpyrrolidone (PVP) (MW = 55K, monomer-based calculation, Sigma-Aldrich, USA) in ethanol solution. Fabricated Cu NWs were stored in ethanol for further use.

Preparation of Ti_3AlC_2 MAX Phase

Preparation and etching of the MAX phase were conducted through the processes which were employed in our previous study[44]. To begin the process, commercially available titanium (Ti), aluminum (Al), and graphite (C) powders were used as the starting materials (Ti and Al: Micron powder, Purity: 99.9%, Nanografi, Turkey and C: Fisher Scientific, USA). Ti, Al, and C powders were mixed in a stoichiometric ratio of 3:1:2 by weight and ball milling was used to mix the powders. A Teflon grinding jar was utilized with zirconia milling balls to assist the milling process with the ball-to-powder weight ratio of 4:1. Once the powders were thoroughly mixed, the resulting mixture was transferred to an alumina crucible. The crucible containing the mixture was then placed inside a tubular furnace, where it was subjected to a continuous argon (Ar) gas flow. The temperature gradually increased at a rate of 5 °C per minute until it reached 1500 °C. The crucible was maintained at 1500 °C for 3 hours to allow for the necessary sintering. Afterward, the furnace was cooled down to room temperature. The resulting MAX phase material was carefully extracted from the crucible and crushed, yielding Ti_3AlC_2 powders.

Preparation of Ti_3C_2 MXene Nanosheets

MXene nanosheets were obtained by dissolving and removing Al from the synthesized MAX phase using a liquid etching process. For this purpose, 3.2 grams of lithium fluoride (LiF) powder (300 mesh, Sigma-Aldrich, USA) was added to a 40 ml solution of hydrochloric acid (HCl) (9 M, Sigma-Aldrich, USA) in a polytetrafluoroethylene (PTFE) beaker. 2 grams of Ti_3AlC_2 MAX powder was gradually added to the LiF-acid solution to avoid overheating caused by the exothermic reactions. The mixture was stirred at a speed of 3500 rpm and maintained at 35°C for 24 hours. After the reaction, the resulting product was washed using deionized (DI) water until the pH of the dispersion reached a neutral level. The delaminated MXene nanosheets were separated from the unreacted MAX phase through subsequent centrifugation and collected as the supernatant. For later use, the concentration of the MXene - DI water dispersion was adjusted to 0.5 mg/ml.

Fabrication of MXene-Cu NWs Transparent Conducting Films

The Cu NWs dispersed in ethanol were deposited onto pre-Ag-contacted poly(ethylene terephthalate) (PET) substrates through spray deposition by a nitrogen-fed airbrush. The substrates were positioned on a hot plate set at 105 °C during the spraying process for the rapid evaporation of ethanol. Afterward, Cu NW deposited electrodes were treated with lactic acid for 10 mins. The lactic acid treatment breaks residual oxides, PVP and HDA on the NWs' surface, improving the conductivity of the network. Afterward, Ti_3C_2 MXene nanosheets were deposited onto Cu NW networks by spin coating at 3600 rpm for 30 seconds to obtain MXene/Cu NW networks. The complete fabrication route of the electrodes is given in Figure 1 (a) with the materials used.

Characterizations

X-ray diffraction (XRD) was conducted using a Rigaku D/Max-2000 diffractometer with Cu Kα radiation at an operating voltage of 40 kV at a scanning rate of 0.1 °/min. X-ray photoelectron spectroscopy (XPS) was conducted by SPECS PHOIBOS instrument and C 1s (at 284.8 eV) was set as a reference. The morphological analysis of the fabricated Ti_3C_2 MXene/Cu NWs was conducted using a field-emission scanning electron microscope (SEM) (Nova NanoSEM 430) at an operating voltage of 20 kV. The optical transmittance measurements of the Cu NW and Cu MXene/Cu NW electrodes were carried out using

Shimadzu UV-3600 within a 380-740 nm wavelength range. Sheet resistances of the fabricated electrodes were measured with Signatone Pro-4 with Keithley 2400 Sourcemeter.

Stability Measurements

The stability measurements of bare and MXene/Cu NW networks were executed by measuring the changes in resistances of the TCEs with TENMA 72-7730 multimeter with its computer monitoring software. The measurement environments were selected as ambient (25 ± 5% average humidity at room temperature), high temperature (75, 100, 125 °C in ambient humidity), and high humidity (75% and 85% relative humidity at room temperature) conditions. High-temperature stability tests were conducted by placing TCEs onto a hot plate which was set to the previously stated temperature for each sample. Relative humidity (RH) conditions of 75% and 85% were achieved in sealed glass jar chambers containing saturated sodium chloride (NaCl) and potassium chloride (KCl) solutions, respectively. An LCD Digital Thermometer Hygrometer Temperature Humidity Meter was used to monitor RH levels during the measurements.

Thin Film Heaters

Heater performance of transparent conducting MXene/Cu NW networks on PET substrates with Ag contacts was monitored by using both thermocouples and thermal cameras. A constant bias was applied to the samples using Nice-Power R-SPS605D DC power supply in the custom-made testing setup. Applent AT4508 Multi-Channel Temperature Meter was used to collect temperature data by connecting two thermocouples (T type copper/constantan) attached to the substrates' backside. The thermal homogeneity of the samples was monitored with the help of the Optris PI 400 thermal camera. To demonstrate defrosting, prepared ice cubes were placed onto the back surface of the MXene/Cu NW electrode (PET side). Digital and thermal cameras have closely monitored the defrosting process until the ice completely melted. In order to demonstrate the thermotherapy application, the MXene/Cu NW electrode was affixed onto the human hand, and the entire process was recorded using the thermal camera. The MXene/Cu NW electrode was heated to 50 °C and cooled back to room temperature during the recording. Written consent was obtained from the user, who attached the heater to their body. The ethics committee approval was obtained from the METU Human Research Ethics Committee (330-ODTUIAEK-2023).

RESULTS AND DISCUSSION

The crystallinity and the purity of the materials which were used to fabricate MXene/Cu NW electrodes are examined with XRD. The results in Figure 1 (b) reveal that the electrode materials, Cu NWs (JCPDS: 03-1018) and $Ti_3C_2T_x$ (JCPDS: 12-0539) MXene, are synthesized successfully. The prominent 2θ peaks observed at 44 and 52° can be attributed to face-centered cubic (FCC) Cu, specifically corresponding to the (111) and (200) crystal planes. In addition to crystallinity, there are no additional peaks belonging to CuO and Cu_2O, indicating the fabrication of highly pure Cu NWs. The peaks on the XRD pattern corresponding to the Ti_3C_2 MXene show the characteristic (002) peak at 7°, which indicates the successful etching of Al from the parent Ti_3AlC_2 MAX phase. No peaks for the MAX phase are observed from the XRD pattern, suggesting the successful fabrication of Ti_3C_2 MXene without any residual MAX phase. XRD analysis for MXene/Cu NWs proves that the electrode materials are synthesized with high purity, yielding high optoelectronic performance.

SEM images of as-prepared bare Cu NWs and MXene/Cu NWs are provided in Figure 1 (c) and (d), respectively. In Figure 1 (c), Cu NWs with ultra-long lengths are observed with an average diameter of 50 nm ± 5 nm. It has been reported that Cu NWs may experience oxide growth in the form of tiny freckle-like spots[45] or mace-like structures[46]. The smooth and continuous shape of nanowires suggests the fabrication of Cu NWs without any oxide species of copper, supporting the XRD results. Figure 1 (d) shows ultrathin Ti_3C_2 MXene nanosheets covering the Cu NW network with various sheet sizes. Elemental maps of the as-prepared MXene/Cu NW network are provided in Figure S1 indicating that MXene nanosheets are located directly on the Cu NWs.

Optoelectronic Performance

In evaluating the optoelectronic performance of the fabricated networks, measurements are conducted to assess both optical transmittance and sheet resistance. The transmittance spectra of bare Cu NWs and MXene/Cu NWs are provided in Figure 1 (e). The total optical transmittance of pristine Cu NWs is 83.7% at a wavelength of 550 nm. Following MXene deposition, the total optical transmittance decreases slightly to 80.5%. Photographs of the bare Cu NW and MXene/Cu NW electrodes are provided in Figure 1 (f) and (g), respectively. Following the deposition of MXene, color neutralization is observed while maintaining a significant level of optical transmittance. As obtained here, this slightly dark gray color is highly desired in optoelectronic devices instead of the reddish color of bare Cu NWs[47].

The electrical performance of the electrodes is determined by means of four-point probe measurements. The sheet resistance of the bare Cu NW film is measured as 29.41 ± 3.15 Ω/sq. Following MXene deposition, the sheet resistance of the MXene/Cu NW film is decreased to 15.05 ± 0.76 Ω/sq. It is worth noting that the MXene deposition also leads to a more uniform sheet resistance across the entire electrode. The change in the optical transmittance and sheet resistance values is expected mainly due to the large MXene sheets spreading across the nanowires, the incident light scatters more and the diffuse transmittance increases as a result. MXene sheets also bridge the gaps between the nanowires and wrap around the nanowire-nanowire junctions. Therefore, the sheets facilitate contact between unattached nanowire ends and reduce the junction resistance[48]. The optical figure-of-merit (FoM), defined as the ratio σ_{DC}/σ_{OP} given by Eq. 1[49] is a useful tool in determining the optoelectronic performance of thin films.

$$\frac{\sigma_{DC}}{\sigma_{OP}} = \left(\frac{188.5}{R_{sh} \times (T^{-\frac{1}{2}} - 1)}\right) \quad \text{Eq. 1}$$

Here, R represents the sheet resistance, T is the optical transmittance, and σ_{DC} and σ_{OP} correspond to the thin film's direct current and optical conductivity, respectively. From Eq. 1, the FoM of bare Cu NW networks is calculated as 68.79 whereas the MXene/Cu NW networks yielded a FoM of 109.2. The improvement achieved in Figure of Merit (FoM) highlights the effectiveness of MXene films in enhancing optoelectronic performance while maintaining optical transmittance without any compromise.

Table 1 provides the studies focused on enhancing the stability of NWs with the materials, production methods, electrical and optical properties, and stability measurements in different conditions. The FoM values are either obtained directly from the text or calculated according to Eq 1. The trade-off between transmittance and sheet resistance can be highlighted and optimizing the two provides a high FoM value. Our work not only has a high FoM among these studies but also constitutes a touchstone with superior stability values obtained in various conditions.

Table 1: Optoelectronic properties of recently published solution-processed highly stable Cu NW networks from literature.

Author (Year)	Material	Production Method	Transmittance (%)	Sheet Resistance (Ohm/sq)	FoM (dc/op)	RH and HT Conditions	RH and HT Stability	Ambient Condition Stability
Wang (2019)[50]	Cu/PMMA/PEDOT:PSS	Spin coating	60	49	13.22	NA	NA	NA
Zhang (2019)[51]	Cu@Ag Core-Shell NWs	Solution based	80	31	51.52	140 °C & 85% RH	500 h	NA
Zhao (2019)[52]	Electroplated Cu NWs	Electrodeposition	83	30	64.35	NA	NA	2 days
Polat Genlik (2020)[30]	BTA/Cu NWs	Solution based	84	31	66.75	75% RH 90% RH 75 °C 120 °C 150 °C	10 days 10 days 250 min 50 min 20 min	1 year
Yang (2020)[53]	AZO/Cu NWs	ALD Coating	87.6	34.05	80.89	120 °C	12 h	NA
Wang (2020)[29]	Graphene/Cu NWs	CVD	84.3	19	111.29	NA	NA	180 days
Zhang (2020)[54]	Cu@Ni Core-Shell NWs	Electrodeposition	88	15.8	180.75	120 °C 400 °C	5h 30 min	NA
Navik (2020)[55]	Cu-Ag Core-Shell NWs	Electroless Ag coating	89	13	241.68	85% RH 85 °C	500 h 500 h	NA
Zhang (2020)[56]	Ag-Au alloy/Cu NWs	Electrodeposition	90.1	14.2	248.09	NA	NA	7 days
Zhang (2021)[57]	Ag-coated Cu NWs	Electrodeposition	90.5	13.8	266.91	NA	NA	7 days
Zhang (2021)[58]	Au/Cu NWs	Electrodeposition	87	23.2	112.67	NA	NA	7 days
Xiang (2022)[59]	Formate-coated Cu NWs	Solution-based	89.19	44.54	71.89	60% RH & 25 °C 85% RH & 60 °C	60 days 5 days	NA
Zhao (2023)[60]	SnO_2/Cu NWs	Solution-based	83.5	13.6	146.90	85% RH & 85 °C	12h	60 days
Dong (2023)[61]	NiO/Cu NWs	Solution-based	84.8	14.9	147.22	85% RH & 85 °C 120 °C	20 h 300 s	30 days
Chiu (2023)[62]	CPI-t/Cu NWs	Spin coating	85	31.69	70.27	NA	NA	90 days
Our Work	*MXene/Cu NWs*	*Solution-based*	*80.49*	*15.05*	*109.27*	*75% RH* *85% RH* *75 °C* *100 °C* *125 °C*	*100 h* *45 h* *600 min* *360 min* *145 min*	*10 months*

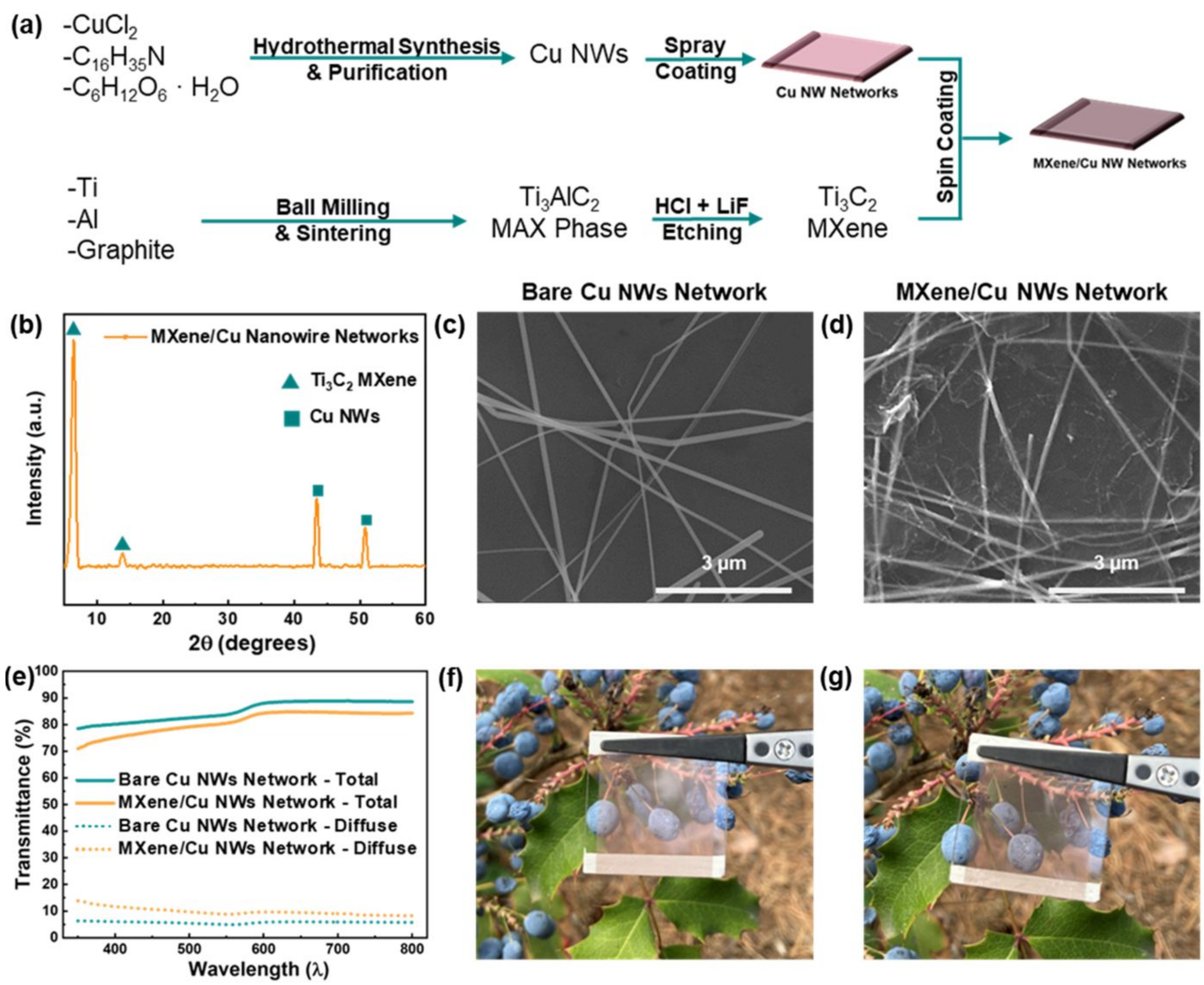

Figure 1: (a) Fabrication of the MXene/Cu NW electrodes and electrode materials (b) XRD pattern of MXene/Cu NW network, SEM images of (c) Cu NW network and (d) MXene/Cu NW network, (e) optical transmittance spectra of Cu NW and MXene/Cu NW networks. Photographs of (f) Cu NW and (g) MXene/Cu NW electrodes.

Ambient Condition Stability

Stability tests are performed first under ambient conditions to evaluate the oxidation stability of MXene/Cu NW electrodes. Over a span of 10 months, variations in relative electrical resistance are observed in both bare and MXene-deposited Cu NW networks. Figure 2 (a) shows the change in the relative resistance for bare Cu NW and MXene/Cu NW networks for 310 days. 10 months after the fabrication of the electrode, the electrical resistance of the MXene/Cu NW electrodes remained constant, while bare Cu NW networks lost their electrical conductivity within 10 days (inset of Figure 2 (a)). SEM images of the Cu NW after 10 days in ambient conditions and MXene/Cu NW networks after 10 months in ambient conditions in Figure 2 (b) and (c), respectively. After 10 days in ambient conditions, the bare Cu NW network is partially broken due to oxidation. The SEM image of the MXene/Cu NW network reveals that the MXene nanosheets act as a protective layer for the Cu NWs. On the other hand, MXene nanosheets experienced partial oxidation because of the presence of atmospheric oxygen in ambient conditions. The partial oxidation of MXene nanosheets reveals that MXene nanosheets provided sacrificial protection for the Cu NWs and electrical conductivity remains preserved even after 10 months. Since the produced Ti3C2 MXenes have very large flake sizes, longer protection time can be achieved as can be seen from the SEM images of the MXene/Cu NWs in the following sections. Small sheet sizes enhance the oxidation behavior of MXene nanosheets since the oxidation starts from the edges of the nanosheets[63]. The partial oxidation of MXene nanosheets can be explained by their surface functional groups (-OH, -F and -O) that form during the chemical etching of Al layers from the parent MAX phase. Oxidation takes place on the MXene nanosheets due to the exchange of surface functional groups with O_2 molecules, facilitated by the weak bonds present[64]. Specific oxide particles on the nanosheets are demarcated with red circles in Figure 2 (c) to aid visual understanding. Underneath the MXene nanosheets, the Cu NWs remain smooth and unoxidized, maintaining their electrical conductivity.

Stability at High Relative Humidity

High levels of humidity serve as an external factor that expedites the corrosion behavior of Cu-based nanomaterials, primarily due to the presence of water molecules.[59] Hence, Cu NWs are susceptible to oxidation when exposed to ambient humidity for extended periods of time. In most optoelectronic applications, the device with Cu NW network operates in ambient conditions, where humidity is crucial in determining the lifetime of the electrode. In order for Cu NWs to be used effectively, corrosion resistance must be increased under ambient humidity conditions. Electrical resistances of both Cu NW and MXene/Cu NW electrodes are monitored to represent their corrosion behaviors under relative humidity levels. To achieve an accelerated degradation of electrodes, they are exposed to high relative humidity (RH) levels of 75% RH and 85% RH. Figure 2 (d) shows the change in the relative electrical resistance over time for Cu NW and MXene/Cu NW electrodes in a 75% RH medium. There is a sudden increase in electrical resistance of the Cu NW electrode after 60 hours due to the high RH level. The SEM image shown in Figure 2 (e) of the degraded bare Cu NW electrode reveals the presence of oxide particles and the accumulation of salts on the surface of the Cu NWs. This accumulation ultimately leads to a complete loss of electrical conductivity. An elemental map for MXene/Cu NW electrode after the test is given in Figure S2, which also proves the Cl^- accumulation to the network. The EDS analysis detects Cl accumulation, and the results are given in Table S1 as the Cl/Ti ratio. Cl/Ti ratio is detected as 0.05 for the freshly prepared Ti_3C_2 MXene, increasing to 2.34 for the MXene/Cu NWs network after the stability test at 75% RH environment. In contrast to Cu NW electrodes, MXene/Cu NW networks remain stable, and no significant change in electrical resistance is observed after exposure to 75 % RH for 100 h (Figure 2 (f)). The regions of the Cu NW networks covered by Ti_3C_2 MXene nanosheets exhibit a lower concentration of oxide particles on the NWs compared to the bare Cu NW network.

The stability measurement results for both Cu NW and MXene/Cu NW networks in 85% RH are given in Figure 2 (g). Bare Cu NW network became electrically non-conductive in less than 25 hours. On the other hand, MXene deposition increases the degradation time to 45 hours. SEM images of both bare Cu NW and MXene/Cu NW networks after exposure to 85% RH for 24.5 hours and 45 hours are given in Figure 2 (h) and (i), respectively. The process of oxidation and the accumulation of ions resulting from salt exposure exhibit similar behavioral characteristics with 75% RH. However, owing to the more severe relative humidity conditions, degradation occurs at an accelerated rate. The regions of Cu NWs coated with Ti_3C_2 MXene nanosheets display a noticeable absence of oxide or salt particles.

The preservation of electrical conductivity in the MXene/Cu NW network under high humidity conditions can be attributed to the deposition of 2D MXene nanosheets, which effectively hinder the interactions between Cu NWs and H_2O molecules in air. The MXene/Cu NW network is subjected to 85% RH environment until a point is reached where electrical conductivity is no longer sustained. Subsequently, XRD analysis was performed on this degraded electrode. The XRD data (Figure S3 (a)), reveals a significant alteration in the crystalline structure of the Ti_3C_2 MXene, as evidenced by the loss of distinct diffraction peaks. Notably, the sole remaining peak observed at 43.52° can be attributed exclusively to the presence of the Cu NWs within the network. As a result, 2D MXene nanosheets act as a sacrificial protective layer to prevent the permeation of the aforementioned molecules to Cu NWs under high RH levels. The performance evaluations of MXene/Cu NW electrodes showed promising potential for their application in optoelectronic devices, even when subjected to high humidity conditions.

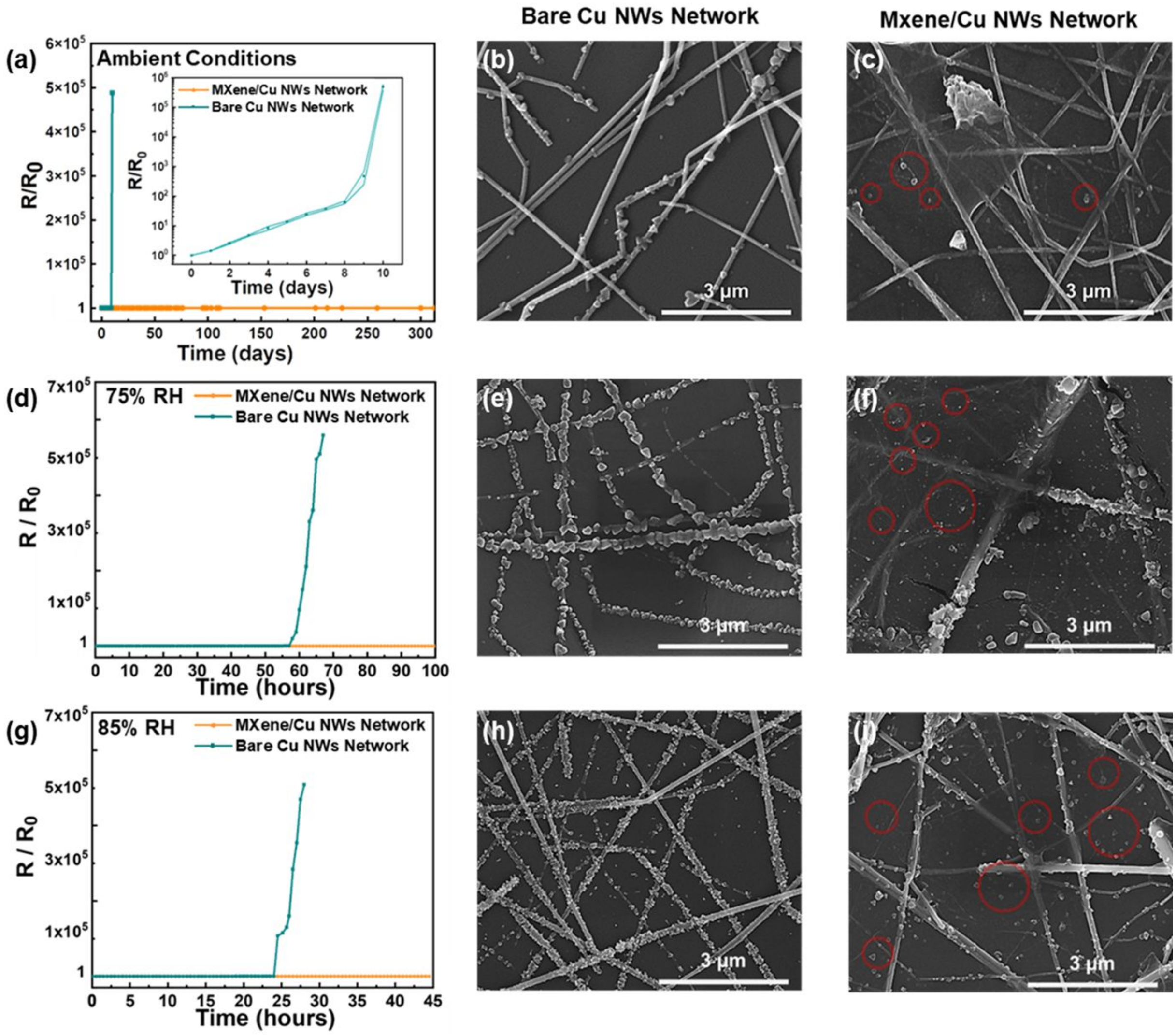

Figure 2: (a) Change in relative resistance of networks under ambient conditions (inset shows changes in relative resistance of bare Cu NW network with error bands). SEM images of (b) Cu NW after 10 days and (c) MXene/Cu NW networks after 5 months, in ambient conditions, (d) change in relative resistance of networks at 75% RH. SEM images of (e) Cu NW and (f) MXene/Cu NW networks after 75% RH stability test. (g) Change in relative resistance of networks at 85% RH, (h) Cu NW and (i) MXene/Cu NW networks after 85% RH stability test (Certain oxide particles on the MXene nanosheets are spotted with red circles).

Stability at High Temperatures

In various applications of Cu NW electrodes, adequate thermal stability is required to preserve electrical conductivity for an extended period. Utilization of Cu NW networks in TTFH applications is challenging due to their poor oxidation stability at elevated temperatures. Thus, enhancing the thermal stability of the Cu NW networks becomes essential to enable their integration into heating devices. In order to compare the thermal stabilities of bare Cu NW and MXene/Cu NW networks, both networks are tested at 75, 100, and 125 °C. Both networks are directly exposed to the selected temperatures in the open atmosphere. Figure 3 (a) shows the change in the electrical resistance of both networks at 75 °C over a period. The resistance of the MXene/Cu NW electrode remained unchanged for 10 hours at 75 °C during the test, which suggests that the exposure of Cu NW networks to oxygen was significantly prevented by the MXene nanosheets. On the other side, when the bare Cu NW electrode was kept at 75 °C, it became non-conductive in less than 200 minutes. Figure 3 (b) shows the SEM image of the bare Cu NW network after the stability test at 75 °C. Due to the high temperature, severe oxide formation on the network occurred, eventually resulting in the loss of electrical conductivity. SEM images of the MXene/Cu NW network after exposure to 75 °C for 10 hours are given in Figure 3 (c). Despite the oxidation occurring on the bare Cu NWs, the regions of the Cu NWs covered by Ti_3C_2 MXene remained unoxidized, effectively preserving the electrical conductivity of the network after 600 minutes. Moreover, the elevated temperatures ended up with the partial oxidation of the MXene nanosheets which were shown in red circles, because of the elevated temperatures. Despite those oxide particles, the electrical conductivity of the network was not severely affected, since the Cu NW network beneath the MXene nanosheets was protected from the ambient oxygen.

Thermal stability tests for both bare and MXene/Cu NW networks are repeated at 100 and 125 °C to investigate the possibility of extended applications of the network at high temperatures. The results are provided in Figure 3 (d), (e) and (f) for 100 °C and (g), (h) and (i) for 125 °C. The lifetime of the electrodes, in terms of electrical conductivity, decreases when the exposed temperature increases from 75 to 100 and 125°C, as given in Figure 3 (a), (d) and (g), respectively. In Figure 3 (b), (e), and (h), it is observed that the sizes of the oxide particles on bare Cu NW networks increase with the temperature. This is because higher temperatures accelerate the growth rate of the oxide particles while slowing down the nucleation rate. These results revealed that the thermal stability of MXene/Cu NW networks substantially outperformed that of Cu NW networks. The mechanism driving this enhancement following

MXene deposition is additionally explored through XRD analysis (Figure S3 (b)) on the MXene/Cu NW network after network decomposition via temperature. The XRD patterns revealed that Ti3C2 MXene is completely decomposed which can be seen from the lack of the peaks belonging to Ti3C2. The sole discernible peaks, located at 44 and 52°, are attributed to the Cu NWs. Therefore, the MXene/Cu NW networks can be considered a promising material to be utilized in optoelectronic applications where high optical transmittance, electrical conductivity, and high-temperature stability are required.

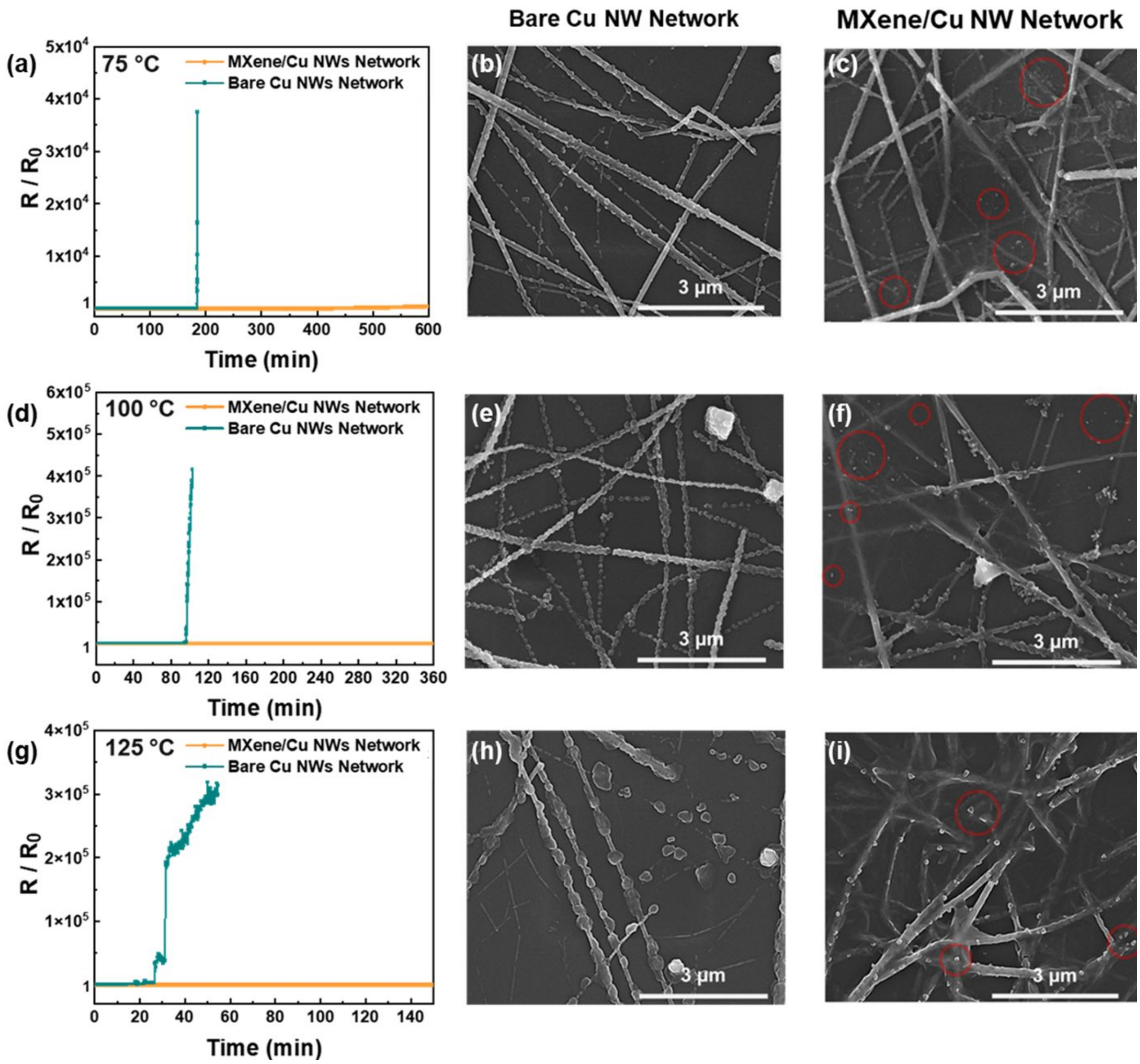

Figure 3: (a) Change in relative resistance of both networks at 75 °C. SEM images of (b) bare Cu NW network after degradation in 75 °C. (c) MXene/Cu NW networks after 600 minutes at 75 °C. (d) Change in relative resistance of both networks at 100 °C. SEM images of (e) bare Cu NW network after degradation at 100 °C. (f) MXene/Cu NW networks after 360 minutes at 100 °C. (g) Change in relative resistance of both networks at 125 °C, SEM images of (h) bare Cu

NW network after degradation in 125 °C. (i) MXene/Cu NW networks after 150 minutes at 125 °C. (Certain oxide particles on the MXene nanosheets are marked with red circles.)

X-Ray Photoelectron Spectroscopy (XPS)

Oxidation properties of the bare Cu NW and MXene/Cu NW networks under ambient, high temperature and relative humidity conditions were investigated through X-ray photoelectron spectroscopy (XPS). First, to understand the protection mechanism of MXene nanosheets at high temperatures both networks were subjected to 125 °C for 10 minutes. Cu 2p spectra of the bare Cu NW and MXene/Cu NWs networks are given in Figure 4 (a) and (b), respectively. Peaks at 932 and 952 eV binding energies represent the metallic Cu whereas the peaks at 933 and 953 eV stand for the oxidized Cu as CuO. It is important to note that the ratio of the total area of Cu^{2+} peaks to the peak areas of Cu^{0} decreased with MXene deposition. This decrease is evidence of the effective protection of Cu NWs from oxidation due to the MXene deposition. Moreover, minor participation of Cu^{+} was distinguished by satellite features at 944 eV, which again has a lower intensity in the MXene/Cu NW network. For further investigation of the protection mechanism of MXene nanosheets, the high-resolution Ti 2p spectra of the annealed MXene/Cu NWs network are presented in Figure 4 (c). Ti $2p_{3/2}$ components are located at 455, 456 and 459 eV standing for the Ti-C, Ti-X (sub-stoichiometric TiC_x) and Ti-O bonds, respectively. Domination of the Ti-O bonds demonstrates the oxidation of the MXene top layer while the Cu NW network underlying has a delayed oxidation behavior (Figure 4(b)) and maintains its electrical conductivity.

Another XPS analysis was conducted to bare and MXene/Cu NW network subjected to high relative humidity conditions to understand the oxidation behaviors. Both samples were exposed to 85% RH for 15 hours. High-resolution Cu 1s spectra for both bare Cu NW and MXene/Cu NW are given in Figure 4 (d) and (e), respectively. In the analysis of the Cu^{2+} peak areas within the networks, a noticeable reduction becomes apparent when examining the MXene/Cu NW network. Additionally, there is a noticeable decrease in satellite features associated with Cu^{+} when MXene was deposited onto the Cu NW network compared to the bare Cu NW network. To investigate the changes in Ti bonds following the RH testing, Figure 4 (f) presents the Ti 2p spectra of the MXene/Cu NW network. Notably, the Ti 2p spectra exclusively exhibit only TiO_2, without T-C and T-X bonds. This lack of T-C and T-X bonds signifies MXene behaving as a sacrificial protection layer for the Cu NW network at high relative humidity conditions.

MXene completely oxidized due to the corrosive environment of high relative humidity conditions while the underlying Cu NW network faced delayed oxidation and maintained its electrical conductivity for a longer time than the bare Cu NW network.

The oxidation behavior of the MXene/Cu NW network in ambient conditions was also examined through XPS analysis. High-resolution XPS spectra for C 1s, Cu 1s, and Ti 2p after one year in ambient conditions are provided in Figure S4. The C 1s and Ti 2p spectra corroborate the complete conversion of Ti_3C_2 into TiO_2, as evidenced by the absence of any peaks associated with titanium carbides and oxycarbides (Figure S4 (a) and (c)). Furthermore, the presence of Cu^0 is reaffirmed by the Cu 1s spectra which confirms the continued electrical conductivity (Figure S4 (b)). The XPS analysis of the electrodes indicates that MXene has undergone full oxidation, whereas the Cu NW network beneath the MXene layer retains its metallic copper composition after a year in ambient conditions. These findings offer that the introduction of MXene acts as an effective sacrificial protective layer for the underlying Cu NW network and blocks the Cu NWs network's access to the oxygen in the air, thus decelerating the oxidation process.

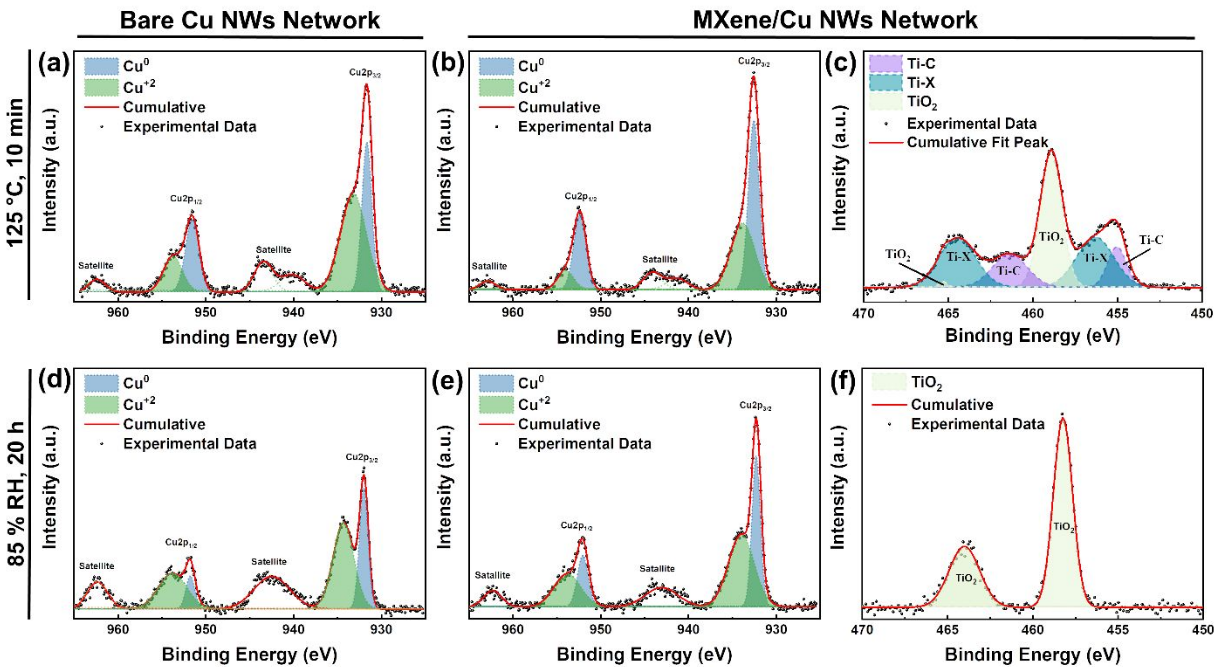

Figure 4: XPS spectra of bare and MXene/Cu NW networks after tested at 125 °C for 10 minutes (a) Cu 1s of bare Cu NW network, (b) Cu 1s of MXene/Cu NW network, (c) Ti 2p of MXene/Cu NW network. XPS spectra of bare and MXene/Cu NW networks after tested in 85% RH for 15 hours (d) Cu 1s of bare Cu NW network, (e) Cu 1s of MXene/Cu NW network, (f) Ti 2p of MXene/Cu NW network.

Transparent Thin Film Heaters

The remarkable optoelectronic properties along with its long-term resistance to oxidation allow MXene/Cu NW electrodes to become promising candidates for TTFHs. In order to confirm the capability of the fabricated TCEs as TTFHs, MXene/Cu NW networks are deposited onto PET substrates and the fabricated electrodes are subjected to a bias voltage of 3 V, increasing their temperature to 50 °C by Joule heating. The linear I-V curve of the electrode given in Figure S5 confirms the Joule heating performance of the network. The long-term stability of the electrodes is carefully monitored, showcasing their durability, while their practicality is demonstrated in applications such as wearable human thermotherapy patches and defrosting electrodes.

The temperatures of both bare and MXene/Cu NW electrodes are monitored to compare their long-term stabilities as TTFHs under 3 V, which caused a temperature increase to 50 °C (Figure 5 (a)). A rapid degradation is observed after 24 hours for bare Cu NW network TTFH. This decrease in temperature is attributed to the increase in resistance as a result of the degradation of the Cu NW electrode. As demonstrated in the previously reported TTFHs, the short-term stability tests might be misleading[65–67]. Therefore, an extensive durability test is conducted for the MXene/Cu NW network TTFH. After 170 hours of durability test, the MXene/Cu NW network TTFH showed extraordinary endurance. Through subjecting the heater to this long-term examination, valuable data is collected to enhance our understanding of its operational lifespan. This meticulous approach enabled us to gather valuable information regarding the durability of the TTFHs. The evidence suggests that TTFHs based on MXene/Cu NW electrodes possess an excellent potential for prolonged use at 50 °C.

Moreover, the temperature distribution of the electrodes at 50 °C is monitored with a thermal camera, images of which are provided in Figure 5 (b-i) and (b-ii) for Cu NW and MXene/Cu NW electrodes, respectively. With the deposition of MXene onto the bare Cu NW network, the temperature distribution under the applied voltage becomes more uniform. This improvement can be attributed to the enhanced percolation of the Cu NWs facilitated by the presence of MXene nanosheets. In addition, the bridging of unattached Cu NWs provides a more uniform Joule heating throughout the electrode. The successful stability results and the achievement of uniform temperature distribution in TTFHs demonstrate the suitability of MXene/Cu NW electrodes for potential real-life applications, including defrosting and human thermotherapy patches.

The successful implementation of a thermotherapy device for medical applications hinges on its capability to uniformly and consistently generate heat when applied to a wound or a specific area of discomfort in the human body. The localized increase in temperature enhances blood circulation, thereby promoting the healing process of wounds and alleviating pain.[68] To utilize TTFHs as thermotherapy devices, electrodes were fabricated on flexible PET substrates to ensure flexibility and conformability to the target area. Electrodes were securely attached to the glove using silver tape and connected to the power supply. Figure 5 (c) shows the heating stages of the thermotherapy device until it reaches 50 °C under an applied voltage of 3 V. The successful utilization of MXene/Cu NW electrodes as TTFHs for human thermotherapy applications is evident in the attainment of the desired temperature on and around the electrodes, even at low bias voltage. This achievement highlights the efficacy of MXene/Cu NW electrodes in providing precise heating for therapeutic applications.

The MXene/Cu NW TTFHs were also employed for defrosting applications for smart windows and car windows. Defrosting electrodes on smart windows are used to eliminate condensation, while the ones on car windows employ embedded heating elements to remove ice or fog for better visibility. An ice cube was carefully placed on the back surface of the electrode and 3 V bias voltage was applied to the electrode to achieve 50 °C by Joule heating. The complete process was followed sequentially by thermal and digital cameras where thermal and digital images are provided in Figure 5 (d). The melting started at the 120th second of the bias voltage application where the object placed under the TTFH became visible as a result of the complete melting of the ice cube after 300 seconds past.

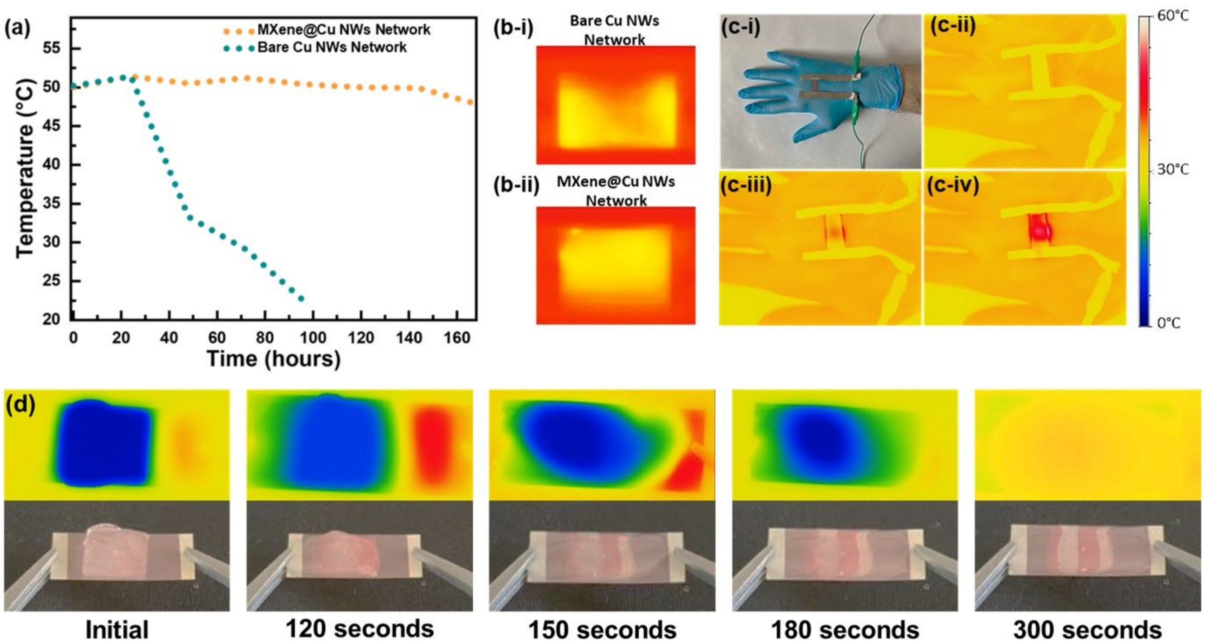

Figure 5: (a) Long-term performance assessment of Cu NW and MXene/Cu NW TTFHs. Thermal camera images for heat distribution under 3 V of the bias voltage of (b-i) Cu NW and (b-ii) MXene/Cu NW thin film heaters. Representation of thermotherapy application by MXene/Cu NW electrode users (c-i) photo, (c-ii, c-iii, c-vi) for the stages of Joule heating under a constant bias voltage of 3 V. (d) Demonstration of defrosting of an ice cube by MXene/Cu NW network TTFHs under 3 V of constant bias voltage.

Cu NWs-based heaters are operational when the stability problems of Cu NW networks are alleviated. For example, Cu-Ni core-shell structures were used to increase the stability of Cu NW networks where the network showed high oxidation stability, but their optical transmittance was low.[69,70] Cu NWs were sandwiched between polymeric materials to produce flexible transparent electrodes with oxidation stability in another work.[71] Additionally, SnO_2-Cu NW networks were also reported as flexible transparent conducting electrodes which were used as heaters.[60] Besides the increased stability of Cu NWs, none of these studies provides any long-term stability assessment for transparent heaters.

The MXene/Cu NW electrodes have successfully demonstrated efficient Joule heating in thermotherapy and defrosting applications. These electrodes possess a high level of oxidation stability, along with prolonged heating performance and uniform heat distribution. Consequently, these findings exhibit tremendous promise for a wide range of transparent heaters and pave the way for further applications that demand high oxidation stability. Compared to other Cu NWs-based heaters, the MXene/Cu NW networks are the first TTFHs observed to maintain their functionality for such an extended period. The long-lasting durability of MXene/Cu NWs in TTFHs introduces a fresh perspective on using heaters for extended periods.

CONCLUSIONS

In this study, we have successfully showcased that the deposition of Ti_3C_2 MXene nanosheets onto Cu NW networks significantly enhances the stability of the conducting network. This enhancement enables their practical use as TTFHs in long-term applications, ensuring their reliability and longevity. MXene/Cu NW networks show improved electrical conductivity without any significant loss in transparency when compared to the bare Cu NW network. This optoelectronic performance improvement carries with the networks' improved stability at high temperatures, in relative humidity and in ambient conditions. This enhanced stability has been confirmed through the continuous measurements of change in the relative electrical resistance under high temperature, in relative humidity and in ambient conditions. The XPS analysis is conducted to investigate the underlying mechanisms behind the improved oxidation stability of the networks and it is understood that MXene nanosheets act as a protective layer for the Cu NW network. MXene/Cu NW networks are utilized as TTFHs through their remarkable optoelectronic performance and improved stability. The successful application of these heaters in human thermotherapy and defrosting provides practical evidence of their effectiveness and successful utilization in real-life scenarios. This showcases their potential for addressing practical heating needs in various applications. The potential of MXene/Cu NW networks was highlighted for a wide range of applications that demand stable and cost-effective electrodes with excellent optoelectronic performance in transparent heating technologies, electrochromic windows, triboelectric nanogenerators and wearable strain sensors.

Acknowledgments

H.E.U. and Y.K. would like to acknowledge the financial support from TÜBİTAK under the 2236-Co-Funded Brain Circulation Program (Project no: 120C065).

Supporting Information

SEM image and EDS map of the MXene/Cu NW networks, XRD patterns and XPS spectra following stability tests, current-voltage characteristic of a MXene/Cu NW network.

REFERENCES

(1) Azani, M.; Hassanpour, A.; Torres, T. Benefits, Problems, and Solutions of Silver Nanowire Transparent Conductive Electrodes in Indium Tin Oxide (ITO)-Free Flexible Solar Cells. *Adv Energy Mater* **2020**, *10* (48), 2002536. https://doi.org/10.1002/aenm.202002536.

(2) Coskun, S.; Selen Ates, E.; Emrah Unalan, H. Optimization of Silver Nanowire Networks for Polymer Light Emitting Diode Electrodes. *Nanotechnology* **2013**, *24* (12), 125202. https://doi.org/10.1088/0957-4484/24/12/125202.

(3) Datta, R. S.; Syed, N.; Zavabeti, A.; Jannat, A.; Mohiuddin, M.; Rokunuzzaman, Md.; Yue Zhang, B.; Rahman, Md. A.; Atkin, P.; Messalea, K. A.; Ghasemian, M. B.; Gaspera, E. della; Bhattacharyya, S.; Fuhrer, M. S.; Russo, S. P.; McConville, C. F.; Esrafilzadeh, D.; Kalantar-Zadeh, K.; Daeneke, T. Flexible Two-Dimensional Indium Tin Oxide Fabricated Using a Liquid Metal Printing Technique. *Nat Electron* **2020**, *3* (1), 51–58. https://doi.org/10.1038/s41928-019-0353-8.

(4) Bae, J.; Seo, D. G.; Park, S. M.; Park, K. T.; Kim, H.; Moon, H. C.; Kim, S. H. Optimized Low-Temperature Fabrication of WO_3 Films for Electrochromic Devices. *J Phys D Appl Phys* **2017**, *50* (46), 465105. https://doi.org/10.1088/1361-6463/aa8e88.

(5) Khademi, S.; Jalili, K.; Wang, H.; Wu, T.; Song, B. Microwave-Assisted Immobilized Silver Nanowires on Arbitrary Substrates: An Eco-Friendly Technique for next-Generation Transparent, Flexible and Robust Electronics. *J Mater Chem C Mater* **2023**. https://doi.org/10.1039/D3TC00742A.

(6) Jang, J.; Parmar, N. S.; Choi, W. K.; Choi, J. W. Rapid Defrost Transparent Thin-Film Heater with Flexibility and Chemical Stability. *ACS Appl Mater Interfaces* **2020**, *12* (34), 38406–38414. https://doi.org/10.1021/acsami.0c10852.

(7) Papanastasiou, D. T.; Schultheiss, A.; Muñoz-Rojas, D.; Celle, C.; Carella, A.; Simonato, J.; Bellet, D. Transparent Heaters: A Review. *Adv Funct Mater* **2020**, *30* (21), 1910225. https://doi.org/10.1002/adfm.201910225.

(8) Li, S.; Tian, M.; Gao, Q.; Wang, M.; Li, T.; Hu, Q.; Li, X.; Wu, Y. Nanometre-Thin Indium Tin Oxide for Advanced High-Performance Electronics. *Nat Mater* **2019**, *18* (10), 1091–1097. https://doi.org/10.1038/s41563-019-0455-8.

(9) Hecht, D. S.; Hu, L.; Irvin, G. Emerging Transparent Electrodes Based on Thin Films of Carbon Nanotubes, Graphene, and Metallic Nanostructures. *Advanced Materials* **2011**, *23* (13), 1482–1513. https://doi.org/10.1002/adma.201003188.

(10) Ye, S.; Rathmell, A. R.; Chen, Z.; Stewart, I. E.; Wiley, B. J. Metal Nanowire Networks: The Next Generation of Transparent Conductors. *Advanced Materials* **2014**, *26* (39), 6670–6687. https://doi.org/10.1002/adma.201402710.

(11) Guo, C. F.; Ren, Z. Flexible Transparent Conductors Based on Metal Nanowire Networks. *Materials Today* **2015**, *18* (3), 143–154. https://doi.org/10.1016/j.mattod.2014.08.018.

(12) Jeon, I.; Yoon, J.; Kim, U.; Lee, C.; Xiang, R.; Shawky, A.; Xi, J.; Byeon, J.; Lee, H. M.; Choi, M.; Maruyama, S.; Matsuo, Y. High-Performance Solution-Processed Double-Walled Carbon Nanotube Transparent Electrode for Perovskite Solar Cells. *Adv Energy Mater* **2019**, *9* (27), 1901204. https://doi.org/10.1002/aenm.201901204.

(13) Eda, G.; Lin, Y.-Y.; Miller, S.; Chen, C.-W.; Su, W.-F.; Chhowalla, M. Transparent and Conducting Electrodes for Organic Electronics from Reduced Graphene Oxide. *Appl Phys Lett* **2008**, *92* (23), 233305. https://doi.org/10.1063/1.2937846.

(14) Hantanasirisakul, K.; Zhao, M.; Urbankowski, P.; Halim, J.; Anasori, B.; Kota, S.; Ren, C. E.; Barsoum, M. W.; Gogotsi, Y. Fabrication of $Ti_3C_2T_x$ MXene Transparent Thin Films with Tunable Optoelectronic Properties. *Adv Electron Mater* **2016**, *2* (6), 1600050. https://doi.org/10.1002/aelm.201600050.

(15) Goak, J. C.; Kim, T. Y.; Kim, D. U.; Chang, K. S.; Lee, C. S.; Lee, N. Stable Heating Performance of Carbon Nanotube/Silver Nanowire Transparent Heaters. *Appl Surf Sci* **2020**, *510*, 145445. https://doi.org/10.1016/j.apsusc.2020.145445.

(16) Yao, S.; Yang, J.; Poblete, F. R.; Hu, X.; Zhu, Y. Multifunctional Electronic Textiles Using Silver Nanowire Composites. *ACS Appl Mater Interfaces* **2019**, *11* (34), 31028–31037. https://doi.org/10.1021/acsami.9b07520.

(17) Cheng, R.; Zeng, J.; Wang, B.; Li, J.; Cheng, Z.; Xu, J.; Gao, W.; Chen, K. Ultralight, Flexible and Conductive Silver Nanowire/Nanofibrillated Cellulose Aerogel for Multifunctional Strain Sensor. *Chemical Engineering Journal* **2021**, *424*, 130565. https://doi.org/10.1016/j.cej.2021.130565.

(18) Doganay, D.; Cicek, M. O.; Durukan, M. B.; Altuntas, B.; Agbahca, E.; Coskun, S.; Unalan, H. E. Fabric Based Wearable Triboelectric Nanogenerators for Human Machine Interface. *Nano Energy* **2021**, *89*, 106412. https://doi.org/10.1016/j.nanoen.2021.106412.

(19) Doganay, D.; Demircioglu, O.; Cugunlular, M.; Cicek, M. O.; Cakir, O.; Kayaci, H. U.; Aygün, S. Ç.; Unalan, H. E. Wet Spun Core-Shell Fibers for Wearable Triboelectric Nanogenerators. *Nano Energy* **2023**, *116*, 108823. https://doi.org/10.1016/j.nanoen.2023.108823.

(20) Zhao, S.; Han, F.; Li, J.; Meng, X.; Huang, W.; Cao, D.; Zhang, G.; Sun, R.; Wong, C.-P. Advancements in Copper Nanowires: Synthesis, Purification, Assemblies, Surface Modification, and Applications. *Small* **2018**, *14* (26), 1800047. https://doi.org/10.1002/smll.201800047.

(21) Manikandan, A.; Lee, L.; Wang, Y.-C.; Chen, C.-W.; Chen, Y.-Z.; Medina, H.; Tseng, J.-Y.; Wang, Z. M.; Chueh, Y.-L. Graphene-Coated Copper Nanowire Networks as a Highly Stable Transparent Electrode in Harsh Environments toward Efficient Electrocatalytic Hydrogen Evolution Reactions. *J Mater Chem A Mater* **2017**, *5* (26), 13320–13328. https://doi.org/10.1039/C7TA01767G.

(22) Li, X.; Wang, Y.; Yin, C.; Yin, Z. Copper Nanowires in Recent Electronic Applications: Progress and Perspectives. *Journal of Materials Chemistry C*. Royal Society of Chemistry 2020, pp 849–872. https://doi.org/10.1039/c9tc04744a.

(23) Wang, J.; Chen, H.; Zhao, Y.; Zhong, Z.; Tang, Y.; Liu, G.; Feng, X.; Xu, F.; Chen, X.; Cai, D.; Kang, J. Programmed Ultrafast Scan Welding of Cu Nanowire Networks with a Pulsed Ultraviolet Laser Beam for Transparent Conductive Electrodes and Flexible Circuits. *ACS Appl Mater Interfaces* **2020**, *12* (31), 35211–35221. https://doi.org/10.1021/acsami.0c07962.

(24) Rathmell, A. R.; Nguyen, M.; Chi, M.; Wiley, B. J. Synthesis of Oxidation-Resistant Cupronickel Nanowires for Transparent Conducting Nanowire Networks. *Nano Lett* **2012**, *12* (6), 3193–3199. https://doi.org/10.1021/nl301168r.

(25) Koylan, S.; Tunca, S.; Polat, G.; Durukan, M. B.; Kim, D.; Kalay, Y. E.; Ko, S. H.; Unalan, H. E. Highly Stable Silver–Platinum Core–Shell Nanowires for H $_2$ O $_2$ Detection. *Nanoscale* **2021**, *13* (30), 13129–13141. https://doi.org/10.1039/D1NR01976G.

(26) Salvatore, K. L.; Deng, K.; McGuire, S. C.; Tan, S.; Rui, N.; Zhang, L.; Rodriguez, J. A.; Wong, S. S. Microwave-Assisted Synthesis of Cu@IrO2Core-Shell Nanowires for Low-Temperature Methane Conversion. *ACS Appl Nano Mater* **2021**, *4* (10), 11145–11158. https://doi.org/10.1021/ACSANM.1C02620/SUPPL_FILE/AN1C02620_SI_001.PDF.

(27) Tigan, D.; Genlik, S. P.; Imer, B.; Unalan, H. E. Core/Shell Copper Nanowire Networks for Transparent Thin Film Heaters. *Nanotechnology* **2019**, *30* (32), 325202. https://doi.org/10.1088/1361-6528/ab19c6.

(28) Won, Y.; Kim, A.; Lee, D.; Yang, W.; Woo, K.; Jeong, S.; Moon, J. Annealing-Free Fabrication of Highly Oxidation-Resistive Copper Nanowire Composite Conductors for Photovoltaics. *NPG Asia Mater* **2014**, *6* (6). https://doi.org/10.1038/am.2014.36.

(29) Wang, J.; Zhang, Z.; Wang, S.; Zhang, R.; Guo, Y.; Cheng, G.; Gu, Y.; Liu, K.; Chen, K. Superstable Copper Nanowire Network Electrodes by Single-Crystal Graphene Covering and Their Applications in Flexible Nanogenerator and Light-Emitting Diode. *Nano Energy* **2020**, *71*. https://doi.org/10.1016/j.nanoen.2020.104638.

(30) Polat Genlik, S.; Tigan, D.; Kocak, Y.; Ercan, K. E.; Cicek, M. O.; Tunca, S.; Koylan, S.; Coskun, S.; Ozensoy, E.; Unalan, H. E. All-Solution-Processed, Oxidation-Resistant Copper Nanowire Networks for Optoelectronic Applications with Year-Long Stability. *ACS Appl Mater Interfaces* **2020**, *12* (40), 45136–45144. https://doi.org/10.1021/acsami.0c11729.

(31) Wang, X.; Wang, R.; Shi, L.; Sun, J. Synthesis of Metal/Bimetal Nanowires and Their Applications as Flexible Transparent Electrodes. *Small* **2015**, *11* (36), 4737–4744. https://doi.org/10.1002/smll.201501314.

(32) Zeng, N.; Fan, S.; Ma, J.; Zhang, Y.; Zhang, S.; Zhang, P.; Zhang, Z. Synthesis and Application of Copper Nanowires and Silver Nanosheet-Coated Copper Nanowires as Nanofillers in Several Polymers. In *Nanowires - New Insights*; InTech, 2017. https://doi.org/10.5772/67782.

(33) Kim, D.; Bang, J.; Won, P.; Kim, Y.; Jung, J.; Lee, J.; Kwon, J.; Lee, H.; Hong, S.; Jeon, N. L.; Han, S.; Ko, S. H. Biocompatible Cost-Effective Electrophysiological Monitoring with Oxidation-Free Cu–Au Core–Shell Nanowire. *Adv Mater Technol* **2020**, *5* (12), 2000661. https://doi.org/10.1002/admt.202000661.

(34) Wang, J.; Du, N.; Zhang, H.; Yu, J.; Yang, D. Cu–Sn Core–Shell Nanowire Arrays as Three-Dimensional Electrodes for Lithium-Ion Batteries. *The Journal of Physical Chemistry C* **2011**, *115* (47), 23620–23624. https://doi.org/10.1021/jp206277a.

(35) Chen, Z.; Ye, S.; Stewart, I. E.; Wiley, B. J. Copper Nanowire Networks with Transparent Oxide Shells That Prevent Oxidation without Reducing Transmittance. *ACS Nano* **2014**, *8* (9), 9673–9679. https://doi.org/10.1021/nn504308n.

(36) E. Stewart, I.; Ye, S.; Chen, Z.; F. Flowers, P.; J. Wiley, B. Synthesis of Cu–Ag, Cu–Au, and Cu–Pt Core–Shell Nanowires and Their Use in Transparent Conducting Films. *Chemistry of Materials* **2015**, *27* (22), 7788–7794. https://doi.org/10.1021/acs.chemmater.5b03709.

(37) Huang, C.-H. ; Lu, Y.-J. ; Pan, Y.-C. ; Liu, H.-L. ; Chang, J.-Y. ; Sie, J.-L. ; Pijanowska, D. G. ; Yang, C.-M.; Lee, J.; Li, M.-Y.; Huang, C.-H.; Lu, Y.-J.; Pan, Y.-C.; Liu, H.-L.; Chang, J.-Y.; Sie, J.-L.; Pijanowska, D. G.; Yang, C.-M. Nanohollow Titanium Oxide Structures on Ti/FTO Glass Formed by Step-Bias Anodic Oxidation for Photoelectrochemical Enhancement. *Nanomaterials 2022, Vol. 12, Page 1925* **2022**, *12* (11), 1925. https://doi.org/10.3390/NANO12111925.

(38) Nosidlak, N.; Jaglarz, J.; Dulian, P.; Pietruszka, R.; Witkowski, B. S.; Godlewski, M.; Powroźnik, W.; Stapiński, T. The Thermo-Optical and Optical Properties of Thin ZnO and AZO Films Produced Using the Atomic Layer Deposition Technology. *J Alloys Compd* **2022**, *900*, 163313. https://doi.org/10.1016/J.JALLCOM.2021.163313.

(39) Yu, H.; He, X.; Liang, X. AlF3-Al2O3 ALD Thin-Film-Coated Li1.2Mn0.54Co0.13Ni0.13O2 Particles for Lithium-Ion Batteries: Long-Term Protection. *ACS Appl Mater Interfaces* **2022**, *14* (3), 3991–4003. https://doi.org/10.1021/ACSAMI.1C20005/ASSET/IMAGES/LARGE/AM1C20005_0011.JPEG.

(40) Shahmohammadi, M.; Mukherjee, R.; Sukotjo, C.; Diwekar, U. M.; Takoudis, C. G. Recent Advances in Theoretical Development of Thermal Atomic Layer Deposition: A Review. **2022**. https://doi.org/10.3390/nano12050831.

(41) Verma, C.; Quraishi, M. A.; Ebenso, E. E.; Hussain, C. M. Recent Advancements in Corrosion Inhibitor Systems through Carbon Allotropes: Past, Present, and Future. *Nano Select* **2021**, *2* (12), 2237–2255. https://doi.org/10.1002/nano.202100039.

(42) Jeong, Y. R.; Park, H.; Jin, S. W.; Hong, S. Y.; Lee, S. S.; Ha, J. S. Highly Stretchable and Sensitive Strain Sensors Using Fragmentized Graphene Foam. *Adv Funct Mater* **2015**, *25* (27), 4228–4236. https://doi.org/10.1002/adfm.201501000.

(43) Santamaría-Juárez, G.; Gómez-Barojas, E.; Quiroga-González, E.; Sánchez-Mora, E.; Quintana-Ruiz, M.; Santamaría-Juárez, J. D. Safer Modified Hummers' Method for the Synthesis of Graphene Oxide with High Quality and High Yield. *Mater Res Express* **2019**, *6* (12). https://doi.org/10.1088/2053-1591/ab4cbf.

(44) Baskoy, M. H.; Cetin, O.; Koylan, S.; Khan, Y.; Tuncel, G.; Erguder, T. H.; Unalan, H. E. MXene-Decorated Nylon Mesh Filters for Improvement of Indoor Air Quality by $PM_{2.5}$ Filtration. *ACS Omega* **2023**. https://doi.org/10.1021/acsomega.3c00452.

(45) Zhai, H.; Wang, R.; Wang, X.; Cheng, Y.; Shi, L.; Sun, J. Transparent Heaters Based on Highly Stable Cu Nanowire Films. *Nano Res* **2016**, *9* (12), 3924–3936. https://doi.org/10.1007/S12274-016-1261-0.

(46) Xu, L.; Yang, Y.; Hu, Z. W.; Yu, S. H. Comparison Study on the Stability of Copper Nanowires and Their Oxidation Kinetics in Gas and Liquid. *ACS Nano* **2016**, *10* (3), 3823–3834. https://doi.org/10.1021/acsnano.6b00704.

(47) Ye, S.; Stewart, I. E.; Chen, Z.; Li, B.; Rathmell, A. R.; Wiley, B. J. How Copper Nanowires Grow and How to Control Their Properties. *Accounts of Chemical Research*. American Chemical Society March 15, 2016, pp 442–451. https://doi.org/10.1021/acs.accounts.5b00506.

(48) Bai, S.; Guo, X.; Chen, T.; Zhang, Y.; Zhang, X.; Yang, H.; Zhao, X. Solution Processed Fabrication of Silver Nanowire-MXene@PEDOT: PSS Flexible Transparent Electrodes for Flexible Organic Light-Emitting Diodes. *Compos Part A Appl Sci Manuf* **2020**, *139*. https://doi.org/10.1016/j.compositesa.2020.106088.

(49) Chen, W.; Zhang, R.; Yang, X.; Wang, H.; Yang, H.; Hu, X.; Zhang, S. A 1D:2D Structured AgNW:MXene Composite Transparent Electrode with High Mechanical Robustness for Flexible Photovoltaics. *J Mater Chem C Mater* **2022**, *10* (22), 8625–8633. https://doi.org/10.1039/d2tc01178f.

(50) Wang, Y.; Liu, P.; Wang, H.; Zeng, B.; Wang, J.; Chi, F. Flexible Organic Light-Emitting Devices with Copper Nanowire Composite Transparent Conductive Electrode. *J Mater Sci* **2019**, *54* (3), 2343–2350. https://doi.org/10.1007/S10853-018-2986-9.

(51) Zhang, B.; Li, W.; Jiu, J.; Yang, Y.; Jing, J.; Suganuma, K.; Li, C. F. Large-Scale and Galvanic Replacement Free Synthesis of Cu@Ag Core-Shell Nanowires for Flexible Electronics. *Inorg Chem* **2019**, *58* (5), 3374–3381. https://doi.org/10.1021/ACS.INORGCHEM.8B03460/SUPPL_FILE/IC8B03460_SI_001.PDF.

(52) Zhao, L.; Yu, S.; Li, X.; Wu, M.; Li, L. High-Performance Flexible Transparent Conductive Films Based on Copper Nanowires with Electroplating Welded Junctions. *Solar Energy Materials and Solar Cells* **2019**, *201*, 110067. https://doi.org/10.1016/J.SOLMAT.2019.110067.

(53) Yang, H.; Kwon, H.-C.; Ma, S.; Kim, K.; Yun, S.-C.; Jang, G.; Park, J.; Lee, H.; Goh, S.; Moon, J. Energy Level-Graded Al-Doped ZnO Protection Layers for Copper Nanowire-Based Window Electrodes for Efficient Flexible Perovskite Solar Cells. *ACS Appl Mater Interfaces* **2020**, *12* (12), 13824–13835. https://doi.org/10.1021/acsami.9b21290.

(54) Zhang, H.; Wang, S.; Tian, Y.; Liu, Y.; Wen, J.; Huang, Y.; Hang, C.; Zheng, Z.; Wang, C. Electrodeposition Fabrication of Cu@Ni Core Shell Nanowire Network for Highly Stable Transparent Conductive Films. *Chemical Engineering Journal* **2020**, *390*, 124495. https://doi.org/10.1016/J.CEJ.2020.124495.

(55) Navik, R.; Ding, X.; Huijun, T.; Zhao, Y. Facile Synthesis of Highly Oxidation Stable Nanosilver-Coated Copper Nanowires for Transparent Flexible Electrodes. *Ind Eng Chem Res* **2021**, *60* (1), 263–272. https://doi.org/10.1021/ACS.IECR.0C04251/SUPPL_FILE/IE0C04251_SI_001.PDF.

(56) Zhang, H.; Tian, Y.; Wang, S.; Huang, Y.; Wen, J.; Hang, C.; Zheng, Z.; Wang, C. Highly Stable Flexible Transparent Electrode via Rapid Electrodeposition Coating of Ag-Au Alloy on Copper Nanowires for Bifunctional Electrochromic and Supercapacitor Device. *Chemical Engineering Journal* **2020**, *399*, 125075. https://doi.org/10.1016/J.CEJ.2020.125075.

(57) Zhang, H.; Wang, S.; Hang, C.; Tian, Y. Joining of Copper Nanowires by Electrodepositing Silver Layer for High-Performance Transparent Electrode. *Welding in the World* **2021**, *65* (6), 1021–1030. https://doi.org/10.1007/S40194-021-01066-7/FIGURES/8.

(58) Zhang, H.; Tian, Y.; Wang, S.; Feng, J.; Hang, C.; Wang, C.; Ma, J.; Hu, X.; Zheng, Z.; Dong, H. Robust Cu-Au Alloy Nanowires Flexible Transparent Electrode for Asymmetric Electrochromic Energy Storage Device. *Chemical Engineering Journal* **2021**, *426*, 131438. https://doi.org/10.1016/J.CEJ.2021.131438.

(59) Xiang, Q.; Navik, R.; Tan, H.; Zhao, Y. Synthesis of Oxidation-Resistance Copper Nanowires-Formate for High-Performance Transparent Conductive Electrodes. *J Alloys Compd* **2022**, *914*, 165265. https://doi.org/10.1016/J.JALLCOM.2022.165265.

(60) Zhao, L.; Li, J.; Song, Z.; Wang, X.; Yu, S. Self-Assembled Growth of SnO2 Nanoshells on Copper Nanowires for Stable and Transparent Conductors. *ACS Appl Nano Mater* **2023**. https://doi.org/10.1021/ACSANM.3C01608.

(61) Dong, H.; Chang, C.; Tan, Q.; Zhao, L.; Yang, P.; Yu, S. Improved Stability of Copper Nanowires with Solution-Grown NiO Shells as Protective Coating. *ACS Appl Nano Mater* **2023**, *6* (12), 10384–10393. https://doi.org/10.1021/ACSANM.3C01329/SUPPL_FILE/AN3C01329_SI_001.PDF.

(62) Chiu, J.-M.; Wahdini, I.; Shen, Y.-N.; Tseng, C.-Y.; Sharma, J.; Tai, Y. Highly Stable Copper Nanowire-Based Transparent Conducting Electrode Utilizing Polyimide as a Protective Layer. *ACS Appl Energy Mater* **2023**. https://doi.org/10.1021/acsaem.3c00703.

(63) Zhang, C. J.; Pinilla, S.; McEvoy, N.; Cullen, C. P.; Anasori, B.; Long, E.; Park, S. H.; Seral-Ascaso, A.; Shmeliov, A.; Krishnan, D.; Morant, C.; Liu, X.; Duesberg, G. S.; Gogotsi, Y.; Nicolosi, V. Oxidation Stability of Colloidal Two-Dimensional Titanium Carbides (MXenes). *Chemistry of Materials* **2017**, *29* (11), 4848–4856. https://doi.org/10.1021/ACS.CHEMMATER.7B00745

(64) Sokolov, A.; Ali, M.; Li, H.; Jeon, Y. R.; Ko, M. J.; Choi, C. Partially Oxidized MXene Ti3C2Tx Sheets for Memristor Having Synapse and Threshold Resistive Switching Characteristics. *Adv Electron Mater* **2021**, *7* (2). https://doi.org/10.1002/aelm.202000866.

(65) Wang, Q. W.; Zhang, H. Bin; Liu, J.; Zhao, S.; Xie, X.; Liu, L.; Yang, R.; Koratkar, N.; Yu, Z. Z. Multifunctional and Water-Resistant MXene-Decorated Polyester Textiles with Outstanding Electromagnetic Interference Shielding and Joule Heating Performances. *Adv Funct Mater* **2019**, *29* (7). https://doi.org/10.1002/adfm.201806819.

(66) Zhou, B.; Han, X.; Li, L.; Feng, Y.; Fang, T.; Zheng, G.; Wang, B.; Dai, K.; Liu, C.; Shen, C. Ultrathin, Flexible Transparent Joule Heater with Fast Response Time Based on Single-Walled Carbon Nanotubes/Poly(Vinyl Alcohol) Film. *Compos Sci Technol* **2019**, *183*. https://doi.org/10.1016/j.compscitech.2019.107796.

(67) Yang, S.; Yan, D. X.; Li, Y.; Lei, J.; Li, Z. M. Flexible Poly(Vinylidene Fluoride)-MXene/Silver Nanowire Electromagnetic Shielding Films with Joule Heating Performance. *Ind Eng Chem Res* **2021**, *60* (27), 9824–9832. https://doi.org/10.1021/acs.iecr.1c01632.

(68) Hossain, M.; Sibin, K. P.; Rao, K. D. M. Angled-Stencil Lithography Based Metal Mesh/Ti3C2T: XMXene Hybrid Transparent Electrodes for Low-Power and High-Performance Wearable Thermotherapy. *J Mater Chem C Mater* **2021**, *9* (19), 6257–6267. https://doi.org/10.1039/d1tc00091h.

(69) Liu, Q.; Tian, B.; Luo, C.; Liang, J.; Wu, W. Printed Flexible Heaters-Based Thermotherapy Platform for Multiduty Thermal Management. *Adv Mater Technol* **2020**, *5* (8), 2000278. https://doi.org/10.1002/ADMT.202000278.

(70) Hazarika, A.; Deka, B. K.; Kim, D.; Jeong, H. E.; Park, Y. Bin; Park, H. W. Woven Kevlar Fiber/Polydimethylsiloxane/Reduced Graphene Oxide Composite-Based Personal Thermal Management with Freestanding Cu-Ni Core-Shell Nanowires. *Nano Lett* **2018**, *18* (11), 6731–6739. https://doi.org/10.1021/ACS.NANOLETT.8B02408/ASSET/IMAGES/LARGE/NL-2018-024089_0005.JPEG.

(71) Kumar, D. V. R.; Koshy, A. M.; Sharma, N.; Thomas, N.; Swaminathan, P. Room Temperature Curable Copper Nanowire-Based Transparent Heater. *ACS Omega* **2023**, *8* (23), 21107–21112. https://doi.org/10.1021/ACSOMEGA.3C02048.